TREAD RUBBER COMPOUND EFFECT IN WINTER TIRES: BENCHMARKING ATIIM 2.0 WITH CLASSICAL MODELS

Mohit Nitin Shenvi*[a], Hoda Mousavi [a], Corina Sandu[a]

[a] *Terramechanics, Multibody, and Vehicle Systems (TMVS) Laboratory*
Department of Mechanical Engineering, Virginia Tech, Blacksburg, VA 24060, United States
mshenvi@vt.edu, hoda13@vt.edu, csandu@vt.edu

* Corresponding Author

This is the Author's Accepted Manuscript (AAM) of:

Shenvi, M. N., Mousavi, H., and Sandu, C. "Tread Rubber Compound Effect in Winter Tires: Benchmarking ATIIM 2.0 with Classical Models." *Journal of Terramechanics*, Volume 101, June 2022, Pages 43-58, https://doi.org/10.1016/j.jterra.2022.02.002

Abstract

Tire-terrain interaction is complex and affects the performance of the vehicle; more so when the terrain is ice which affects the handling of the vehicle. Analysis of the contact between the tire and ice, especially in the countries like United States, Canada, etc. is imperative but a trial-and-error approach consisting of the design and manufacture of novel tires for testing and analysis seems a foregone conclusion. Thus, it is important to have accurate methods of simulation of tire performance on ice in order to design better tires without inputting much cost in the manufacturing process.

This study chose to simulate the performance of sixteen tires which were identical in all aspects of design and construction except for the tread rubber compound which varied resulting in two tires having the same tread rubber compound. These simulations were performed using the in-house developed ATIIM, ATIIM 2.0, and modified versions of three simplified classical models namely the model by Hayhoe and Shapley and two models by Peng et al. A qualitative comparison of the performance of the models was performed in order to highlight their advantages and disadvantages.

Keywords: Tire-ice model, dry friction, fluid friction, water film height, tread rubber compound, winter tires

---

Nomenclature

h(x)	Height of water film	[m]	L	Normal Load	[N]
ρ	Density of ice	[kg/m^3]	H	Latent heat of ice	[J/kg]
v	Velocity of sliding	[m/s]	k,λ	Thermal conductivity of ice	[Wm^{-1}K^{-1}]
ΔT_{m-i}	Difference in initial and melting temperature of the ice	[°C]	T_b	Ice bulk temperature	[°C]
C_p	Specific heat capacity	[J/kgK]	μ	Friction coefficient	[]
σ_n	Normal Stress	[MPa]	ΔT	Rise in temperature	[°C]
P_{avg}	Nominal contact Pressure	[MPa]	A	Aggregate application	[gm/m^2]
t_c	Contact time	[s]	α	Thernal diffusivity of ice	[m^2/s]

1. Introduction

For the majority of the vehicles, the part which creates or alters relative motion between the vehicle and the surface is the pneumatic tire. The terrains can generally be classified into two subtypes namely rigid terrains (asphalt, ice, etc.) or deformable terrains (soil, snow, sand, etc.). On a rigid terrain like ice, the reliance on the skills of the driver increases as the available friction at the tire-ice interface reduces, which can be attributed to several factors related to the ice as well as the tire.

In the USA, approximately 70% of roadways face a mean annual snowfall of greater than 5 inches (US. Department of Transportation, 2020). This existence of snow or ice on re-crystallization on the road impacts the handling behavior leading to a high number of accidents, even with the presence of a skilled driver. On an average 156,164 crashes and 521 fatalities occurred every year from 2007 to 2016 due to such conditions (US. Department of Transportation and Administration, 2020). These numbers provide an endorsement for additional research in the tire-ice contact phenomenon. A reduction in the dependency on driver skills could be attained by improving the tire design. However, manufacture and

in-field testing of candidate tires will not always prove to be cost-efficient, providing an impetus to the development of accurate simulation approaches replicating the results from experimental testing. The current study is an attempt to computationally study the effect of variation in tread rubber compound on the performance of winter tires on ice.

For this, the choice of a set of sixteen tires (in subsets of two per rubber compound), identical in all aspects of design and construction, except for the rubber compound of their tread was performed. The tests for evaluation of the pressure distribution of the tires were performed on an indoor rig consisting of a single wheel tester (Sandu et al., 2008) at the Terramechanics, Multibody, and Vehicle Systems Laboratory (TMVS). A prior study in the lab (He et al., 2017) for tire-ice testing has also included parametrization of the Dugoff Tire Model using data obtained from the tests performed in the rig. To focus only on the effect of the tread rubber compound all experimental parameters were kept constant. These collected pressure distributions were then evaluated using in-house developed ATIIM (Jimenez and Sandu, 2018), ATIIM 2.0 (Mousavi and Sandu, 2020a, 2020b, 2020c) and suitable modifications were made to three classical models (Hayhoe and Shapley, 1989; Peng et al., 2000, 1999) to benchmark the overall applicability against each other and experimental results.

This document is further subdivided into sections. Section 2 consists of a detailed review of relevant literature along with the explanations of the classical models. Section 3 details the design of experiments, material properties, and various steps followed for the preparation of the tires. Section 4 includes the results from the simulations by the various models and specific findings from this process and a comparison to the experimental findings of this study wherever applicable. Section 5 lists the conclusions and directions for future work in this area of research.

2. Review of relevant literature

In this section, the literature related to the tire-ice contact phenomenon, the effects of the various parameters on the performance of tires found in the literature are presented along with an explanation of the classical models of tire-ice contact used in this study.

2.1 Introduction to the tire-ice contact phenomenon and the importance of tread rubber

The classical laws of friction fail to provide a comprehensive understanding of the friction mechanism of tires, which is mostly attributed to the higher pressures at the interface (Moore, 1975). The friction mechanism at the tire-terrain interface is primarily attributed to the adhesion and sliding phenomena. If the road surface has a layer of water or the

presence of ice or snow, the more dominant adhesion component is reduced significantly (Blundell and Harty, 2004). The experimental investigation on the effects of surface roughness of rubber by using two types of rubber samples having identical properties except for surface roughness (Xu et al., 2013) revealed that the friction of the textured rubber sample was higher in the low-speed region (<0.1 m/s) when the surface was lubricated but this trend reversed when the speeds were higher due to amplification in the water film formation and presence of the micro-cavitation effect.

Ice as a terrain increases the complexities in the friction analysis even more which is due to presence of a quasi-liquid layer of melted ice which has low shear strength (Nakajima, 2019). This fluid layer will increase further if the velocity of the rubber block or normal load (pressure at contact) increases as it will increase the heat generated contributing to more melting of ice and an increase in water film height which in turn will reduce the friction available (Wallaschek and Wies, 2013). Thus, the most crucial parameters dominating the friction at the tire-ice interface are the velocity, normal load, and temperature of the ice.

The shortcomings of all-season and summer tires in cold or icy conditions boosted the development of technology for winter-specific tires. The earlier variant called studded winter tires is not much in use primarily due to damage to the asphalt in non-wintry conditions and the issue of noise. The improvement in rubber compounding and tire siping technology led to a boost of studless winter tires with the salient features of more sipes, characteristic design of tread pattern, greater tread depth, and type of rubber compound used. The working of the tire makes clear that the tread is the part in contact with the terrain and thus the properties of the tread rubber will be more influential in the performance of a tire on ice as they will dictate the relative interaction. Amongst the features of winter tires, the depth of tread and specific design of tread pattern will vary between the manufacturers which leaves the improvement in performance to two factors namely sipes and tread rubber compound. Amongst these Ripka et al's (Ripka et al., 2012) findings proved that the sipes per tread block would also reach an optimum as far as friction improvement is concerned as shown in Figure 1. Hence, for further improvement in winter tires, it seems obvious to study the tread rubber compound effect.

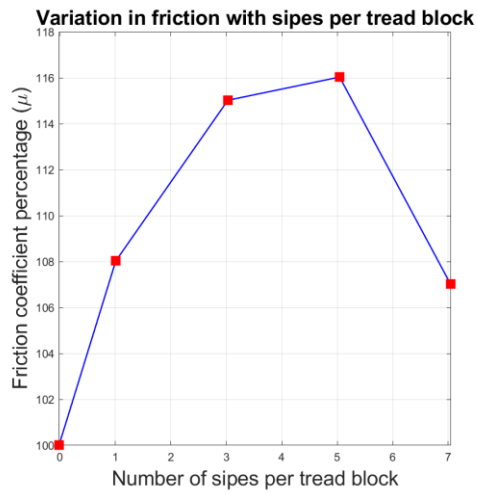

Figure 1: Variation in the coefficient of friction with a change in the number of sipes. Redrawn in agreement to the plot in (Ripka et al., 2012)

2.2 Effects of rubber compound on the rubber-ice friction

Persson (Persson, 2006), found that the flash temperature dictates the friction mechanism when velocity is greater than 0.01 m/s in the context of rubber-asphalt friction. In a logical extension of this finding, this role would be even more prominent when the terrain is ice as it would lead to an increase in the localized melting of ice. Another work (Tuononen et al., 2016) uses a multiscale physics-based approach to evaluate the rubber-ice friction phenomenon. The authors found that the tread rubber's viscoelastic dissipation while sliding on ice asperities has a notable contribution on the ice friction in the 0.001-1 m/s velocity range.

The experimental investigation of the rubber-ice friction phenomenon (Skouvaklis et al., 2012) revealed that temperature and sliding velocity had an inverse relation with the coefficient of friction which was due to their effect on the melting of ice and a resultant increase/decrease in the water layer present. The friction at lower speeds was found to be mostly influenced by the viscoelastic properties of rubber leading to a conclusion that the rubber which was softer had a greater friction coefficient as exhibited in Figure 2.

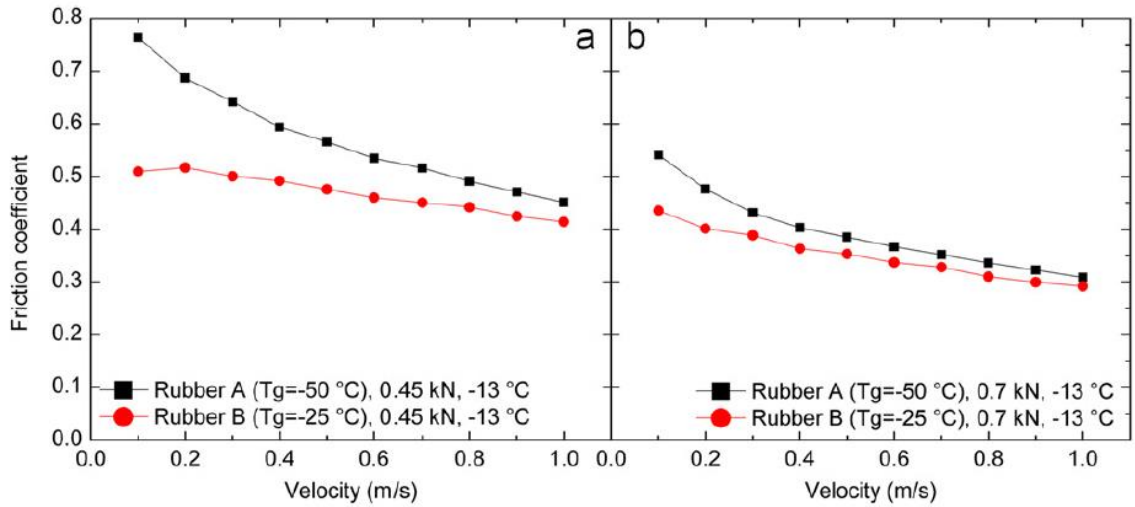

Figure 2: Comparison of the coefficient of friction for two rubbers with different properties. Reprinted from (Skouvaklis et al., 2012) with permission of Elsevier

The work of Klapproth et al (Klapproth et al., 2016), developed a viscous model for investigating rubber-ice friction. It investigated the effect of various parameters like sliding velocity, nominal pressure, the temperature of ice, the stiffness of the rubber, etc. The study found that though in general, the softer rubber compounds have greater friction, this trend reversed when the contact pressures were high leading to the harder rubber compound having a higher friction coefficient. Other studies like Isitman et al (Isitman et al., 2017) too found an inverse relationship between the dynamic friction coefficient and rubber stiffness. Yamazaki et al (Yamazaki et al., 2000) concluded that at lower velocities or when the temperature is nearing the melting point of ice the effect of sipes is negligible, hence this effect was neglected in our work but could be a factor introducing variations.

2.3 Classical approaches to modeling tire-ice friction

Some of the prior attempts at analyzing tire-ice friction have taken various factors into consideration and have improved over the years. A model developed by Higgins et al (Higgins et al., 2008), based on the unsteady heat flow equation calculates the time required for the temperature of ice to reach the melting point. A modified formulation presented by the authors in their work (Skouvaklis et al., 2012) could be described as shown in eqn. (1)

$$\mu = \frac{\Delta T_{m-i}}{2v\sigma_n}\sqrt{\lambda C_p \rho}\sqrt{\frac{\pi}{t_c}} \tag{1}$$

where μ is the coefficient of friction, ΔT is the difference in the initial and melting temperature of the ice, σ_n is the normal pressure, v is the sliding velocity, λ is the thermal conductivity of the ice, C_p is the specific heat capacity, ρ is the density of ice, and t_c is the duration for which the rubber slides against a specific position on the surface of the ice. The model developed by Lahayne et al (Lahayne et al., 2016) was based on an experimental investigation of three different rubber compounds on four types of ice surfaces with 3 levels of normal load and 4 levels of ambient temperature, and a fixed sliding velocity. This model is capable of including the effect of roughness of ice which affects the value of friction as shown in Table 1, for one such rubber compound (R_2) at -13°C ambient temperature and nominal pressure of 0.3 MPa.

Table 1
Coefficient of friction values depending on ice surface roughness. Adapted from (Lahayne et al., 2016)

Type of Ice	Measured value of the coefficient of friction
I_1	0.435
I_2	0.378
I_3	0.5
I_4	0.576

A model for evaluation of friction coefficient incorporating the effects of ambient temperature and aggregate material was developed by Navin et al (Navin et al., 1996). Two equations were developed considering a car and a truck tire as shown in eqns. (2) and (3), where 'T' refers to the temperature in °C whereas '*A*' refers to the aggregate material application in gm/m^2. The major drawback of this model would be that even if we assume the accuracy of friction evaluation to be high, the model would estimate similar values of friction as long as the amount of aggregate application and ambient temperature is constant. Thus, the variation that change in aggregate material would offer cannot be estimated by this model which was highlighted by Bhoopalam et al (Bhoopalam et al., 2014), in which the peak normalized drawbar pull attained using different aggregates varied largely.

$$\mu(ice, car) = 0.11 - 0.0052\,T + 0.0002\,A \tag{2}$$

$$\mu(ice, truck) = 0.10 - 0.0052\,T + 0.00016\,A \tag{3}$$

Evans et al (Evans et al., 1976) developed an analytical model for evaluating ice friction, albeit in the context of ice skating, but the principle basically suggested that the heat generated due to force of friction (F_f) can be subdivided into three contributions namely, the heat conducted through the ice (F_i), the heat conducted through the body (F_r) and the heat

required to melt the ice (F_m). The final equation for friction evaluation is as shown in eqn. (4), where 'A' and 'B' are constants that depend on the area, geometry of material, thermal properties of ice, and dimensions of the contact patch, 'L' is the normal load applied, and 'T_m' and 'T_o' are the melting and ice surface temperatures respectively. The contribution of 'μ_m' was found to be negligible in most of the cases but a major drawback of this model is that the evaluation of the constant 'A' is not clear.

$$\mu = \frac{Ak(T_m - T_o)}{Lv} + \frac{B(T_m - T_o)}{Lv^{\frac{1}{2}}} + \mu_m \tag{4}$$

Further, three classical models were chosen to be evaluated in comparison to the in-house models as described in subsequent subsections. The choice of the classical models (Hayhoe and Shapley, 1989; Peng et al., 2000, 1999) was performed primarily due to the usage of the same type of properties that are required by the in-house models and the ease of computation that the classical models allow due to some of the inherent assumptions. The evolution of the in-house models is directly or indirectly based on the classical models chosen which would lead to interesting perspectives when comparing the findings. Also, the classical models chosen provide a capability of evaluation the point where frictional melting of ice occurs which would be of scientific interest given that it would distinguish the regimes of dry and wet friction theoretically.

2.3.1. Hayhoe and Shapley model

An analytical model developed by Hayhoe and Shapley (Hayhoe and Shapley, 1989), proposed that the contact patch between tire and ice could be divided into two regions namely the leading part consisting of dry sliding and the trailing part having a fluid water film contributing to viscous friction. Major assumptions of this model were: a smooth tire surface, constant pressure in the contact patch, no heat flow into the tire (as the thermal conductivity is much less than ice), and heat flow from the contact interface is linear in the vertical direction. The work also proposed the concept of transition point which is shown in Figure 3.

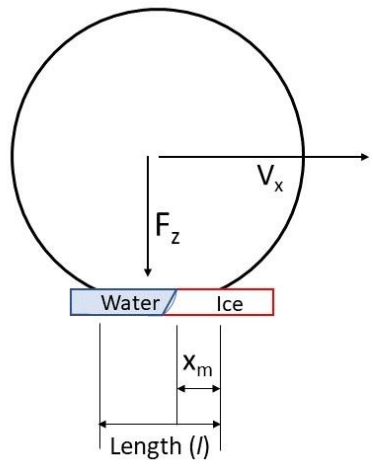

Figure 3: Separation of the dry and wet sliding regions of tire on ice. Redrawn in agreement to (Hayhoe and Shapley, 1989)

Eqn. (5) evaluates the change in temperature at the interface between the tire and ice. As the authors assume that the conductivity of the rubber is zero, this evaluation of temperature rise is solely dependent on the numerator of eqn. (5). This assumption won't be able to predict the effect of different rubber compounds while evaluating rise in temperature and hence eqn. (6) was developed by considering the conductivity of rubber, where the distance '*x*' is considered to be a product of velocity '*v*' and time '*t*'. If the melting point of ice is assumed to be 0°C, the rise in temperature will be equal to the magnitude of the bulk temperature of ice, which helps in evaluating the distance of transition point from the leading edge of the contact patch, according to eqn. (7). The estimation of friction forces in the current work follows the approach in (Hayhoe and Shapley, 1989), except for neglect of viscous friction coefficient in the cases where transition point lies outside the length of the contact patch indicating no occurrence of melting.

$$\Delta T = \frac{\frac{2\,\dot{Q}_S}{k_{ice}} \cdot \left[\frac{\alpha_{ice} \cdot t}{\pi}\right]^{0.5}}{\frac{k_{rubber}}{k_{ice}} \cdot \left[\frac{\alpha_{ice}}{\alpha_{rubber}}\right]^{0.5} + 1} \tag{5}$$

$$\Delta T = \frac{\frac{2\,\dot{Q}_S}{k_{ice}} \cdot \left[\frac{\alpha_{ice}}{\pi \,.\, v}\right]^{0.5} \cdot x^{0.5}}{\frac{k_{rubber}}{k_{ice}} \cdot \left[\frac{\alpha_{ice}}{\alpha_{rubber}}\right]^{0.5} + 1} \tag{6}$$

$$x_m = \left[\frac{k_{ice} \cdot T_b}{2\,\dot{Q}_S} \cdot \left(\frac{k_{rubber}}{k_{ice}} \cdot \left[\frac{\alpha_{ice}}{\alpha_{rubber}}\right]^{0.5} + 1\right)\right]^2 \cdot \frac{\pi \,.\, v}{\alpha_{ice}} \tag{7}$$

2.3.2. Models by Peng et al.

Peng et al developed two analytical models in consecutive years (Peng et al., 2000, 1999) to analyze the friction mechanism at the tire-ice interface. Most of the assumptions in both of these models are inspired from the model explained in section 0. The models are developed for the rectangular as well as the elliptic condition of the contact patch. For evaluation of the friction in this work, formulations related to rectangular contact patch are considered. The earlier model consisted of estimating the water film height by solving a fourth-degree polynomial equation, which is then used to calculate the friction in the contact patch. Drawback of this procedure, however, is that a single value of the height of water film does not make physical sense, even if the estimated height of water film increases with an increase in slip ratio as expected. As the earlier model (Peng et al., 1999) evaluates the transition point from the lagging edge of the contact patch, as in Figure 4, the transition point is calculated using eqn. (8). The transition point and other physical properties are used to evaluate the three constants shown in eqn. (9). These three constants are used to calculate the height of water film according to eqn. (10), which in turn is used to calculate the average value of friction coefficient according to eqn. (11). Appropriate changes to this procedure were made to account for the condition where no melting occurs.

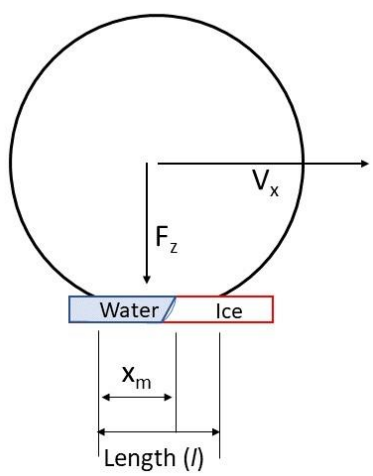

Figure 4: Transition point from dry sliding to melted water film under a tire moving on ice. Redrawn in agreement to (Peng et al., 1999)

$$x_m = length - \left(\frac{\pi v}{\alpha_{ice}}\right)\left(\frac{T_b k_{ice} C}{2\dot{Q}_s}\right)^2 \tag{8}$$

$$C_1 = \eta V_{sliding}^2 \,;\, C_2 = 2T_b(C_t + C_{ice})\left(\frac{U}{x_m}\right)^{\frac{1}{2}};\quad C_3 = \frac{p_{avg}\rho H}{\eta . width^2} \tag{9}$$

$$C_1 - C_2 h - C_3 h^4 = 0 \tag{10}$$

$$\mu_{avg} = \mu_s\left(1 - \frac{x_m}{l}\right) + \frac{\eta V_{sliding}}{h\,.\,p_{avg}}\left(\frac{x_m}{l}\right)^2 \tag{11}$$

The latter model developed by the authors bypassed the step of estimation of water film height for the prediction of friction coefficient and calculated the transition point from the leading edge of the contact patch. This model utilizes the contact patch dimensions, normal load, bulk ice temperature, thermal properties of ice and tread, and the sliding velocity for estimating the value of transition point, fluid friction coefficient, and average friction coefficient as shown in eqns. (12), (13), and (14) respectively. In these equations, the constant 'C_b' is dependent on the thermal properties of the tread rubber and the ice.

$$x_m = \left[\frac{\pi C_{ice} C_b T_b}{4\mu_d p_{avg} V_{sliding}}\right]^2 V_{axle} \tag{12}$$

$$\mu_f = \frac{C_{ice} C_b T_b}{p_{avg}\sqrt{length\,.V_{sliding}}} \tag{13}$$

$$\mu_{avg} = \mu_d\left(\frac{x_m}{l}\right)^2 + (C_{ice} + C_{tread})T_b\left(1 - \frac{x_m}{l}\right)^{\frac{3}{2}}\left(\frac{l}{V}\right)^{-\frac{1}{2}}\left(P_{avg}.V_{sliding}\right)^{-1} \tag{14}$$

2.4 In-house developed models (ATIIM and ATIIM 2.0)

The Advanced Tire-Ice Interface Model (ATIIM) was developed (Jimenez and Sandu, 2018) as an improvement over the Tire-Ice model (Bhoopalam et al., 2016) which served to calculate the temperature rise using Jaeger's temperature rise formulation, according to the finite difference formulation developed by Fujikawa et al (Fujikawa et al., 1994). The success of this model was in the computation of the viscous friction coefficient by differentiating the areas of dry and wet contact. The required inputs along with the pressure distribution of the tire contact were the density, thermal conductivity, and specific heat capacity of the tire and the tread rubber. The drawback of this model however was too much focus on the viscous friction effect and the less number of relevant rubber physical properties considered.

To overcome this drawback, ATIIM 2.0 was developed by Mousavi and Sandu (Mousavi and Sandu, 2020a). The algorithm of the model inititally calculates the change in temperature based on the two-dimensional pressure distribution in the contact patch, the mechanical and thermal properties of the tread rubber, the interactional properties like sliding velocity, and the properties of ice. Further the rise in temperature is used to evaluate the height of the water film created by frictional heating. This is used to evaluate the viscous and dry friction coefficients and subsequently the

equivalent friction coefficient. The model includes the incorporation of the squeeze-out term as well as computation of the height of water film from a time-dependent version to a length-dependent version (Mousavi and Sandu, 2020a; Wiese et al., 2012). The model captures the effects of various parameters (density, thermal conductivity, and specific heat of the rubber) that are already a part of ATIIM and also incorporates the effect of the complex Young's modulus, and surface roughness distribution (by a combination of average radius of spherical asperities and roughness parameter of rubber) on the prediction of water film height and friction. A comprehensive description of the model and material parameters for the ATIIM and ATIIM 2.0 is found in literature (Mousavi and Sandu, 2020a). Ideally the measurement of the surface roughness distribution should be performed after the tire wear process for experimental testing (Shenvi et al., 2022). However, as the equipment required for such an exercise were not readily available, the values of surface roughness distribution were assumed based on findings in literature. The authors also validated the model experimentally (Mousavi and Sandu, 2020b) as well as performed a sensitivity analysis (Mousavi and Sandu, 2020c) to evaluate the extent to which the individual parameters affect the computation of the friction coefficient.

3. Design of experiments, material properties, and data collection methodology

3.1 Design of experiments for collection of pressure distribution

The design of experiments was created in order to purely focus on the tread rubber compound of the tires. The chosen values of normal load and inflation pressure were 4000 N and 28 psi respectively. The camber and toe angles were kept at 0°. The design of experiments table was modified in comparison to the experimental testing DOE table as the pressure measurement system faced issues of damage at higher slip ratios due to shearing. The design of experiments for pressure distribution measurement is shown in Table 2. There were total of 8 different tread rubber compounds named from A-H however, their compositional variations were not disclosed by the sponsoring agency. Thus, an attempt was made to find the effect of the variations on the tire performance and contact patch friction based on the mechanical properties of the rubber that were available and detailed in section 3.2. The choice of the DOE variables chosen are described in the article focusing on the experimental work of the study (Shenvi et al., 2022).

Table 2
Design of experiments

	Rubber comp. A	**Rubber comp. B**	**Rubber comp. C**	**Rubber comp. D**	**Rubber comp. E**	**Rubber comp. F**	**Rubber comp. G**	**Rubber comp. H**

Tire	Tire A1	Tire A3	Tire B1	Tire B3	Tire C1	Tire C3	Tire D1	Tire D3	Tire E1	Tire E3	Tire F1	Tire F3	Tire G1	Tire G3	Tire H1	Tire H3
Load (kN)	4	4	4	4	4	4	4	4	4	4	4	4	4	4	4	4
Infl. Pres. (psi)	28	28	28	28	28	28	28	28	28	28	28	28	28	28	28	28
Slip ratio	0%, 2%, 4%, 6%, 8%, 10%, 12%, 15%, Free Rolling															

3.2 Material Properties

In the review of literature conducted as a part of this and the supporting work (Shenvi et al., 2022), it was found that the density and stiffness of the rubber compounds were found to be most prominent in the effect on rubber-ice friction. However, in order to have a more in-depth study, the water film generated and its effects on the contact patch friction regime need to be studied which would be possible by consideration of the thermal conductivity (which is low for rubbers) and specific heat capacity (which would govern the amount of heat flowing into the tire) for all the rubber compounds. The exact composition of the rubber compounds was not disclosed, hence only the physical and thermal properties of the rubber were considered for the simulation purposes as all the models require this data as input. Further, some assumptions were made for simulation purposes in case a specific property was not available and interpolation of material property value was performed if necessary as the temperature of simulation study varied from the temperatures at which the rubber material properties were evaluated.

1. **Density of rubber compound**: The density of tread rubbers of the tires varied from the lowest at 1094 kg/m^3 for rubber compound C up to the highest at 1157 kg/m^3 for the rubber compound H, as shown in Table 3.

Table 3
Density of the rubber compounds

Rubber Compound	**Density (kg/m^3)**
A	1105
B	1103
C	1094
D	Not Available
E	1104

F	1139
G	1137
H	1158

2. **Thermal conductivity**: As the thermal conductivity of the rubber is comparatively much less than the thermal conductivity of ice, it was assumed to be constant for all the rubber compounds at 0.3 $Wm^{-1}K^{-1}$.

3. **Specific heat capacity** (J/(g.K)): The specific heat capacity at different temperatures was available for 5 of the rubber compounds. Its values at three levels of temperature are shown in Table 4.

Table 4
Excerpt of the specific heat capacity values of the rubber compounds at different temperatures

Temp. (°C)	A	B	C	D	E	F	G	H
-5	Not Available	1.84	2.03	2.09	Not Available	2.18	2.09	Not Available
0		1.88	2.14	2.26		2.28	2.26	
5		1.92	2.18	2.29		2.30	2.29	

4. **Stiffness properties**: The storage modulus, loss modulus, dynamic modulus, and the tangent of the phase angle between the storage and loss modulus were known at various temperatures for several rubber compounds. The values of these three properties at some temperatures are shown from Table 5-Table 8.

Table 5
Storage modulus at different temperatures for various rubber compounds

Temp (°C)	E' (in MPa)							
	A	B	C	D	E	F	G	H
-5.6	Not Available	3.495	4.556	Not Available	Not Available	Not Available	6.489	7.977
-2.7		3.401	4.197				6.184	7.568
0.4		3.137	4.153				6.03	7.115

Table 6
Loss modulus at different temperatures for various rubber compounds

Temp (°C)	E'' (in MPa)							
	A	B	C	D	E	F	G	H

-5.6	Not Available	0.808	0.839	Not Available	Not Available	Not Available	1.115	1.669
-2.7		0.765	0.771				0.992	1.54
0.4		0.587	0.762				0.983	1.328

Table 7
Dynamic modulus of rubber at different temperatures for various rubber compounds

Temp (°C)	**E* (in MPa)**							
	A	**B**	**C**	**D**	**E**	**F**	**G**	**H**
-5.6		3.587	4.633	Not Available			6.584	8.149
-2.7		3.486	4.268				6.263	7.723
0.4	4.21	3.191	4.222		5.26	4.87	6.11	7.238

Table 8
Tangent of phase angle at different temperatures for various rubber compounds

Temp (°C)	**tanδ**							
	A	**B**	**C**	**D**	**E**	**F**	**G**	**H**
-5.6	Not Available	0.231	0.184	Not Available	Not Available	Not Available	0.172	0.209
-2.7		0.225	0.184				0.16	0.204
0.4		0.187	0.184				0.163	0.187

3.3 Description of pressure distribution measurement system and test method

The pressure measurement system used at the TMVS lab is the Tekscan 3150 pressure measurement system. The pressure pad has 2288 sensels spaced equally apart in rows and columns providing a pressure sensing area of 160759.22 mm^2 and a spatial resolution of about 1.4 sensels/cm^2 (Tekscan Inc., 2018). Before testing, the pressure pad needs to be equilibrated i.e. applied a uniform pressure in order to confirm that all the sensors sense equally well when uniform pressure is applied. This process is also helpful to detect faulty rows or columns of sensels which could happen due to overuse or shearing effect as time progresses.

This is followed by the calibration of the pressure pad by application of a known load usually in the vicinity of the target normal load on the tire. Misiewicz et al. (Misiewicz et al., 2015) developed a multi-point per sensel method for calibration of the pressure measurement products of Tekscan (although their tests did not include the system used in the TMVS lab). The authors were successful in reducing the bias and statistical errors by about 66% in comparison to the

proprietary method of calibration. The pressure measurement performed for this study, however, was performed after the recommended calibration method suggested by the manufacturer.

Before measurement of pressure distribution the tire break-in process was performed (ASTM F1805-20, 2020). In order to avoid damage to the pressure pad, it was covered with a Photodon 6HS Tempered Glass film. This method, however, only delays the emergence of faulty sensors depending on how strongly the film is fixed to the base. In order to pass the pressure distribution as an input to the ATIIM and ATIIM 2.0 models, the data needs to be zero-padded in the regions outside of the contact patch. Sometimes due to damage, an array of sensors (mostly perpendicular to tire movement direction), do not detect the pressure as a black line in the lateral direction of the contact patch, as shown in Figure 5. Interpolation of data is performed in such a case to compute the possible values that would have been recorded by the sensors. This emergence of fault lines occurs over repeated use of pressure pad due to squeezing of pressure pad at high slip ratios as shown in Figure 6. This is the reason the pressure distribution was curtailed at 15% slip ratios. Another method to remedy this was the removal of the pressure pad after daily use to avoid it from getting stuck to the protective film due to high pressures during testing.

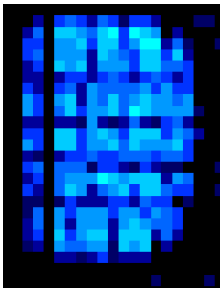

Figure 5: Faulty array of sensors in a specific run of a tire over the pressure measurement system when the tire moves from left to right

Figure 6: Squeezing of the pressure distribution setup when a tire is rotating with 12% slip ratio

4. Simulation results and discussion

This section details the results of simulations performed by using the properties of the tire available using various models explained in sections 2.3.1, 2.3.2, and 2.4.

4.1 Results for the rise in temperature (ATIIM)

The rise in temperature based on the pressure distribution data collected for all the tires was simulated using ATIIM. The specific heat properties of rubber compound G were used for rubber compounds A, E, and D. It was also assumed that rubber compound D had a density equivalent to rubber compound F. The results of the simulations for 4% slip ratio are presented in Table 9. The assumed static friction coefficient for the simulations was 0.1, as this was ensured to be the static friction coefficient of ice during experimental testing. A significant point was that the emergence of wet regions due to a rise in temperature overcoming the difference between bulk ice temperature and melting point did not initiate till approximately 10% slip ratio. For the simulations presented, the tire moved from the left to right and the highest temperature rise occurred as the tread progressed from the leading edge towards the trailing edge. Another significant point was that the highest temperature rise was also observed on tread blocks near the periphery of the contact patch in the lateral direction in some cases.

Table 9
Rise in temperature simulation for all the tires at 4% slip ratio using ATIIM

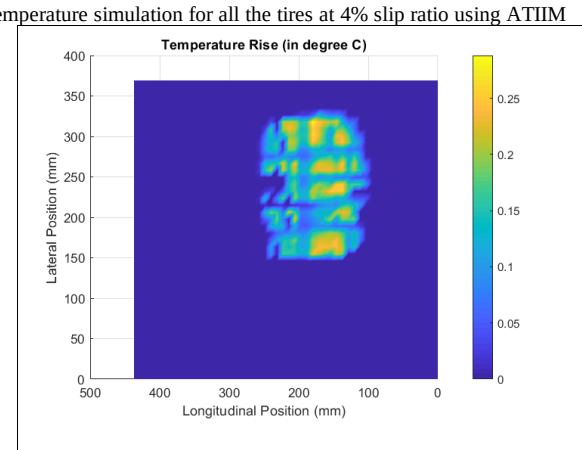	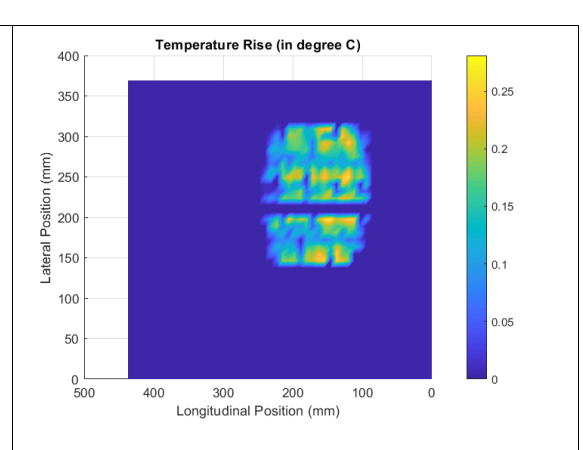
Tire A1	Tire A3

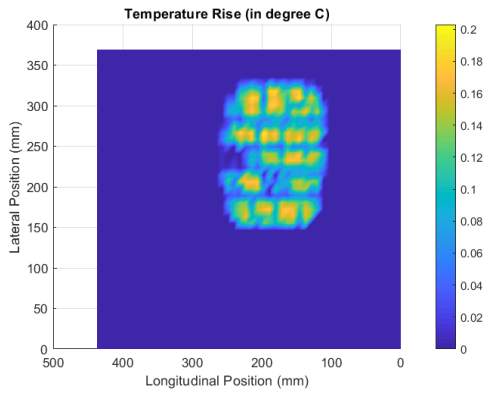

Tire B1

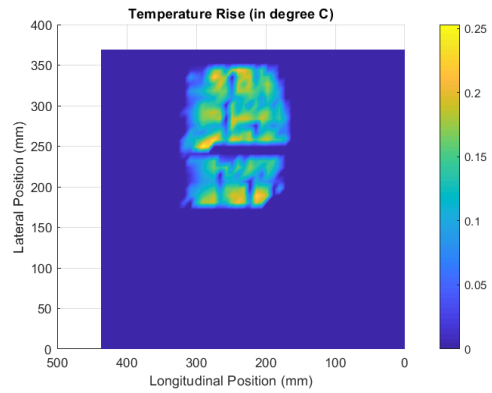

Tire B3

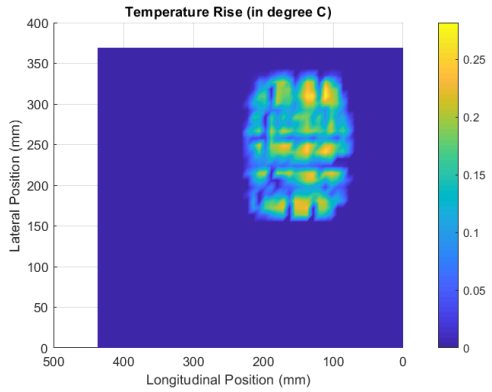

Tire C1

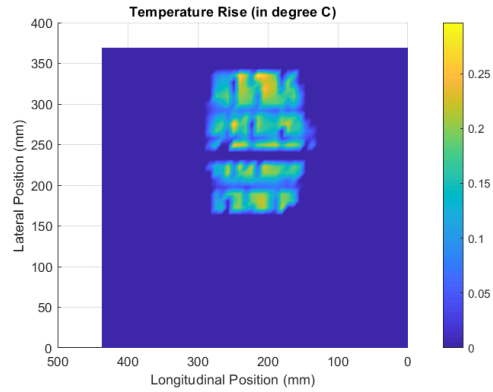

Tire C3

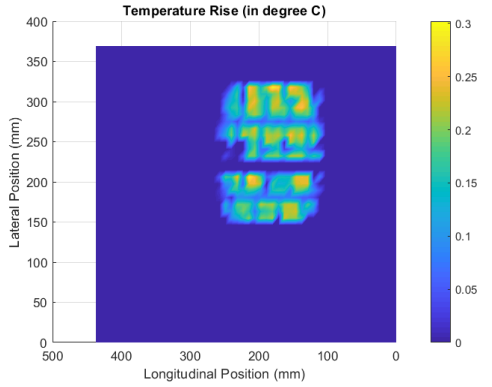

Tire D1

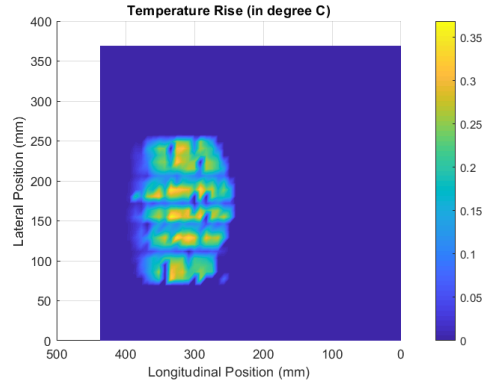

Tire D3

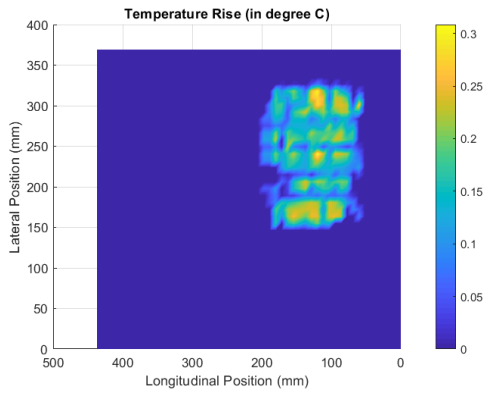

Tire E1

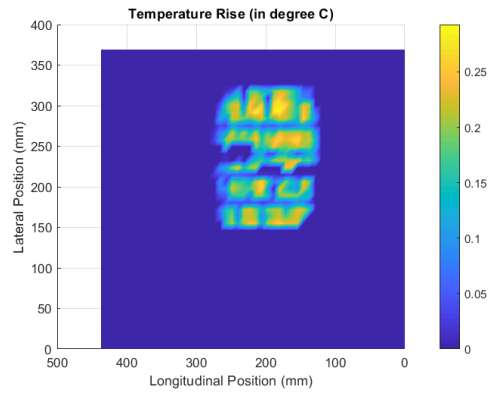

Tire E3

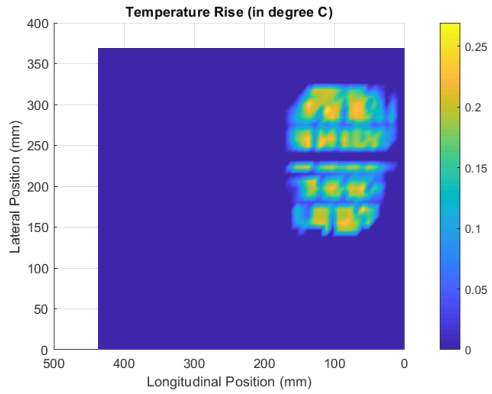

Tire F1

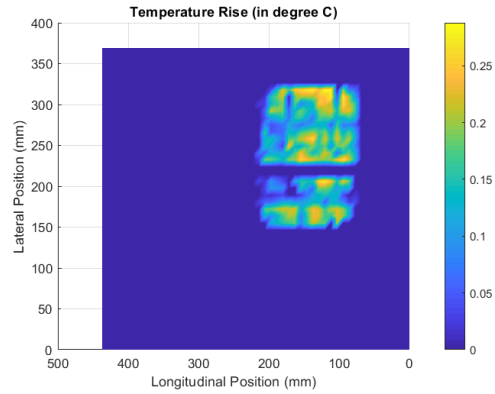

Tire F3

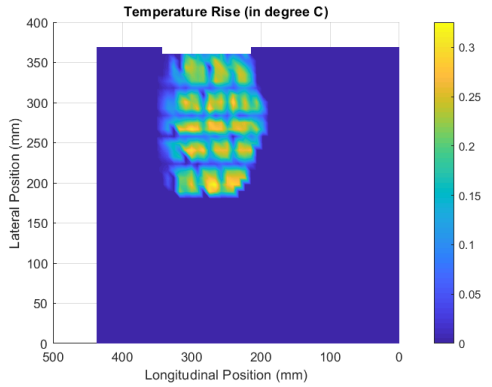

Tire G1

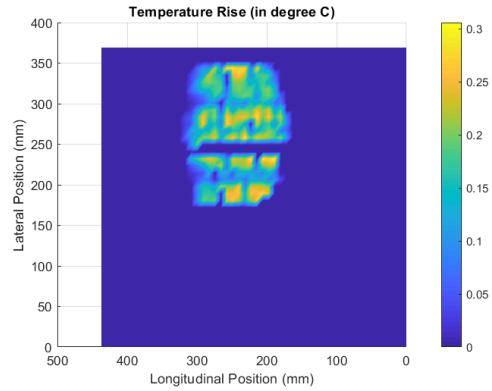

Tire G3

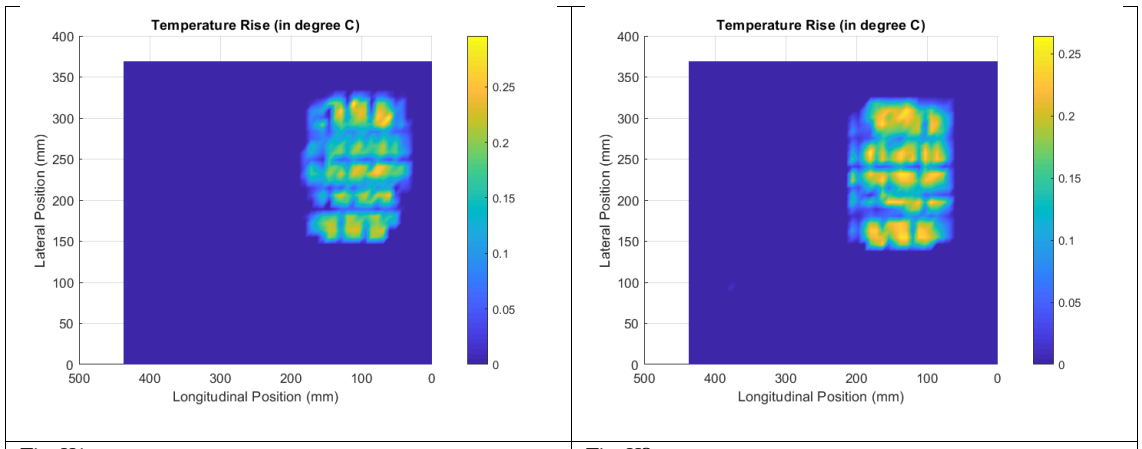

Tire H1	Tire H3

4.2 Results for water film height (ATIIM 2.0.)

Computation of water film height was conducted using ATIIM 2.0. As the physical property (density) of rubber compound D was not available, simulations for the rubber compound D were not run as it would imply a lot of assumptions of properties. The values of the roughness parameter ($l_r = 6.5\ \mu m$) and mean root square gradient ($\nabla z = 0.35$) were taken from available values in literature (Wiese et al., 2012). The computed height of water film at 4% slip ratio for all the tires is shown in Table 10. Some conclusions from the simulations are

1. With an increase in the slip ratio, the height of the water film estimated increases for all the tires. This generalized trend is seen irrespective of the rubber compound wherein the rubber compound effect only affects the average height as well as maxima of the water film.
2. Variations were seen in the predicted height of water film for two tires of the same rubber compound, even without the aging effect which could be due to some of the assumptions about the properties of rubber compounds, roughness parameters, etc., or due to variations in the pressure distribution measured.

Table 10
Estimated height of water film for all tires simulated using ATIIM 2.0 in 4% slip ratio configuration

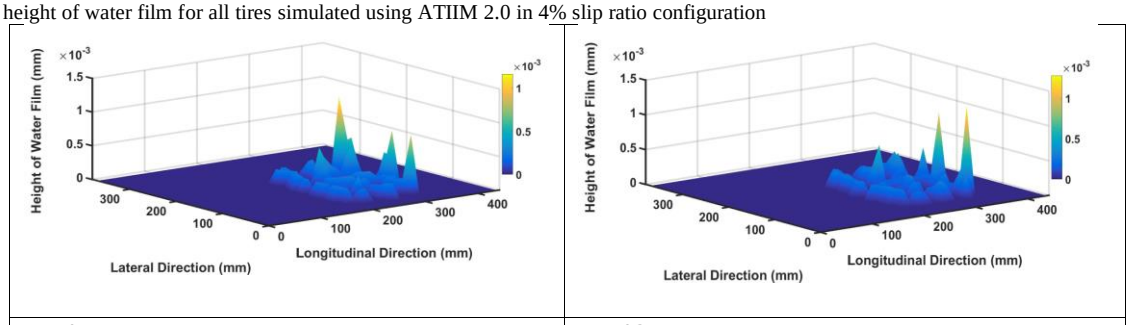

Tire A1	Tire A3

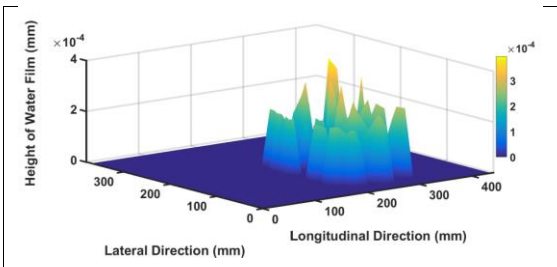

Tire B1

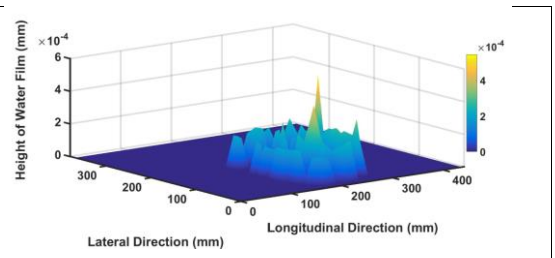

Tire B3

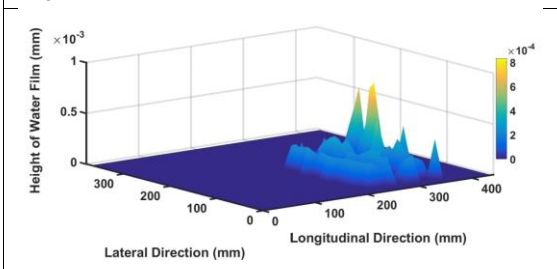

Tire C1

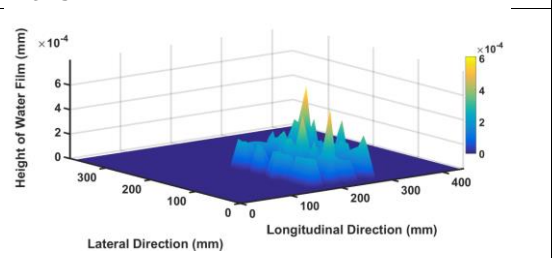

Tire C3

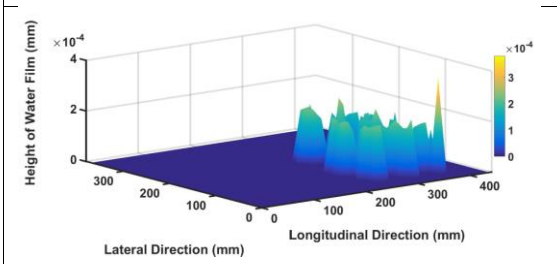

Tire E1

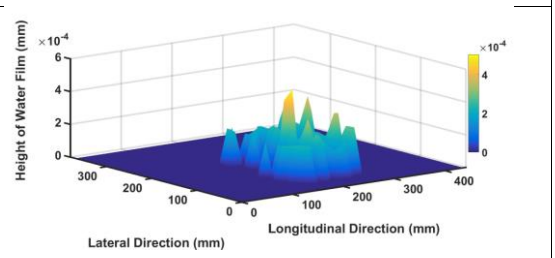

Tire E3

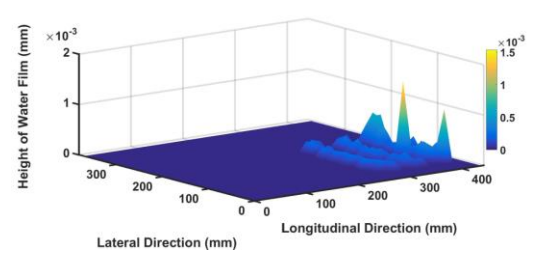

Tire F1

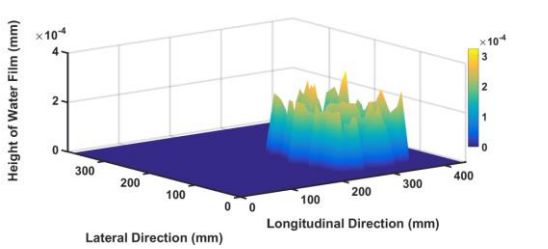

Tire F3

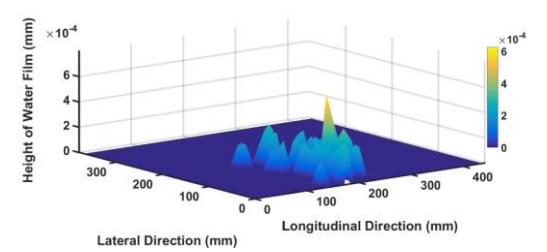

Tire G1

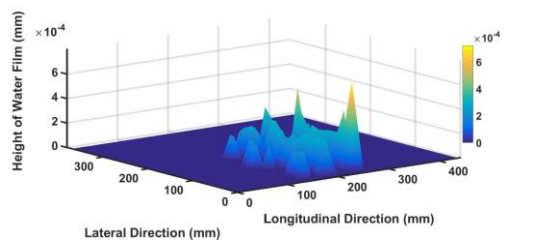

Tire G3

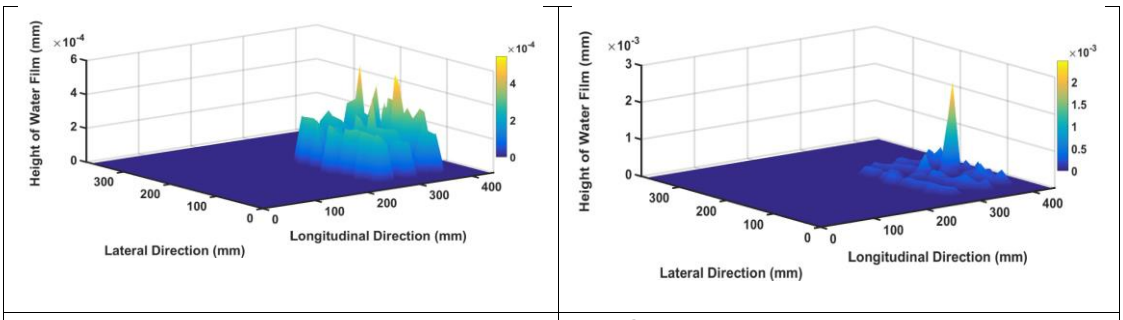

Tire H1	Tire H3

4.3 Predictions of the Hayhoe and Shapley model

Appropriate changes were made to the original model (Hayhoe and Shapley, 1989), to be able to visualize the effect of the rubber compounds. Firstly, this meant overriding the assumption that no heat flows into the tire. Secondly, in the cases where the predicted point of transition by this theory lied outside the limit of the contact patch, the fluid friction coefficient estimated was equated to be zero. The distance of the point of transition from the leading edge is shown in Figure 8. A rise in slip ratio leads the point of transition to move towards the leading edge of the contact patch i.e. the region of dry sliding reduces which also has an effect on the reduction of the overall coefficient of friction. The model is successful in predicting more rise in temperature as the distance from the leading edge increases (Figure 9) but fails to capture the temperature rise along the lateral direction as well as the effect that the tread pattern, a characteristic of winter tires, can have on the temperature rise. The prediction of friction coefficient using this model (Figure 7), is supportive of the conclusion from experimental results that the variance in friction coefficient is highest in the low slip region whereas in the higher slip region, irrespective of the rubber compound, the value tends to be in a small range of each other. Another similarity to the experimental results lies in the highest-ranked rubber compound (H), which highlights the important role played by the density of tread rubber in the tire-ice contact phenomenon. The predicted order of total friction coefficient according to this model is: **H>F>D>G>A>E>C>B**

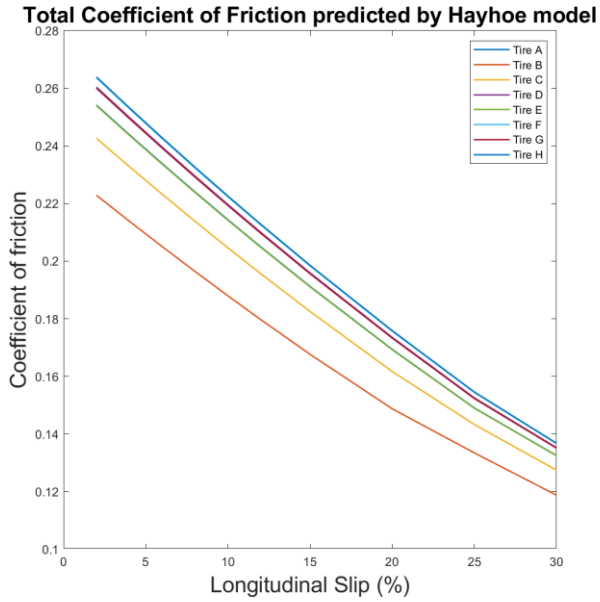

Figure 7: Total coefficient of friction prediction by Hayhoe and Shapley model

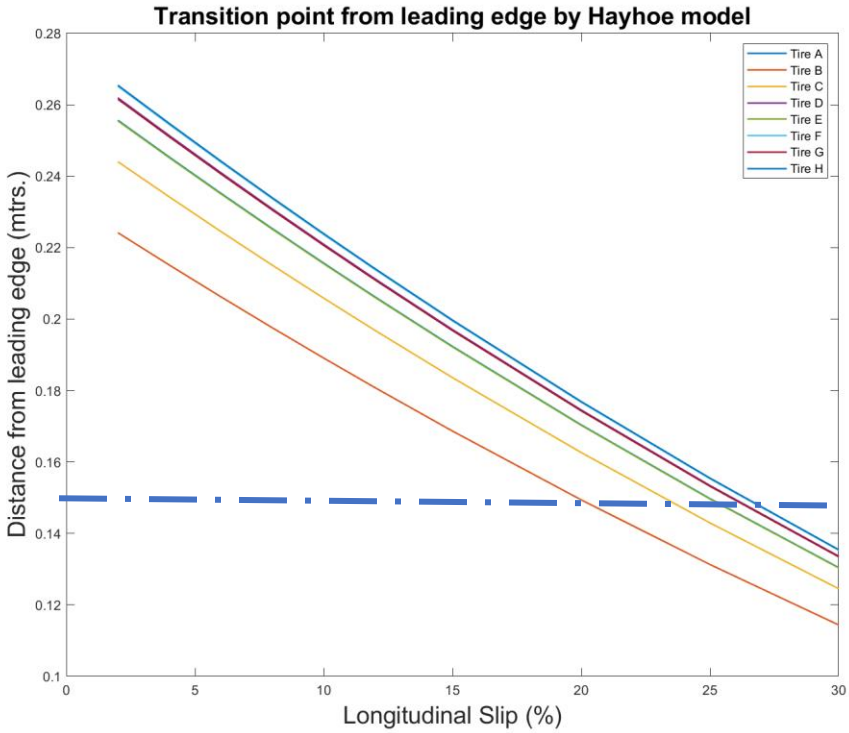

Figure 8: Variation in point of transition for all tires with a change in slip ratio for Hayhoe and Shapley model

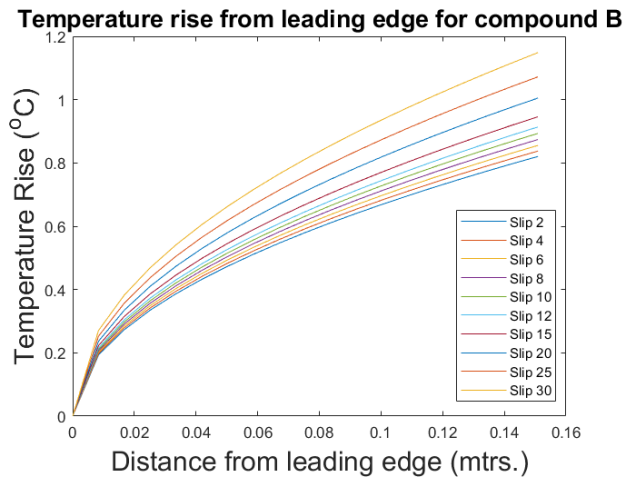

Figure 9: Temperature rise for rubber compound B by simulation using Hayhoe and Shapley model

4.4 Predictions of the 2nd Peng et al. model

The latter model developed by Peng et al. does not estimate the height of water film before estimating the friction coefficients. The point of transition occurred outside the contact patch in some cases even with this model. Similar to the predictions of the Hayhoe and Shapley model, the transition point moved towards the leading edge (Figure 12) with an increase in slip ratio, due to an increase in the fluid friction region but the value of the fluid friction coefficient (Figure 10) according to this model reduced with an increase in slip ratio which is in contradiction to the findings of most studies in this region of research. The average friction coefficient had an inverse relation with the slip ratio as expected (Figure 11). The predicted order of total friction coefficient according to this model is: **H>F>D>G>A>E>C>B**

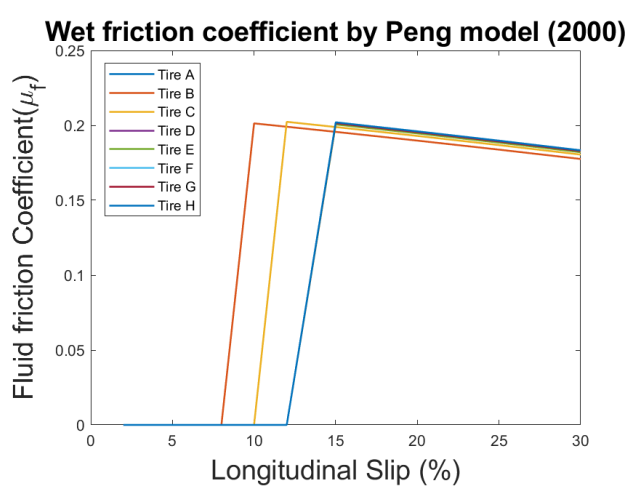

Figure 10: Coefficient of fluid friction predicted by the 2nd Peng model

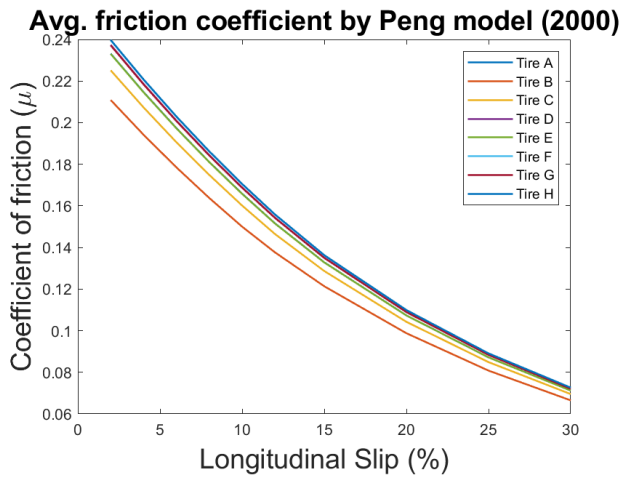

Figure 11: Average coefficient of friction predicted by 2nd Peng model

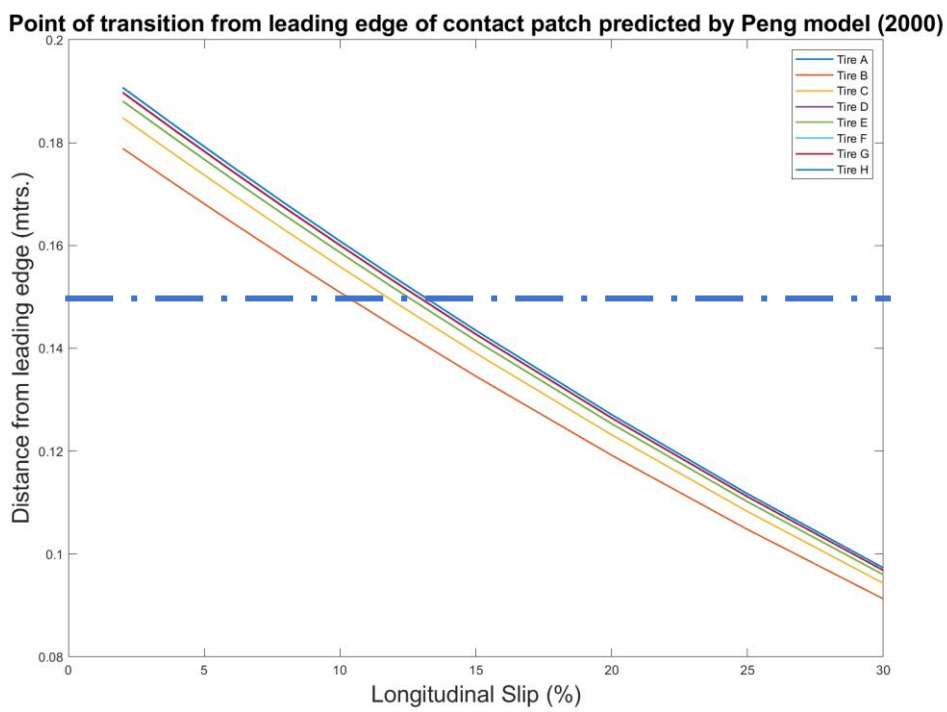

Figure 12: Point of transition prediction by 2nd Peng model

4.5 Predictions of the 1st Peng et al model

The earlier Peng et al model calculated the transition point from the trailing edge of the contact patch. Even by the use of this model, there were occurrences of the transition point (Figure 16) being outside the contact patch, however,

even with the different method of calculating the transition point, both the Peng et al models predict the initiation of melting at around 8% - 12% slip ratio range, varying based on the rubber compound. If the model predicted non-occurrence of melting, changes were made in order to have the height of water film (Figure 13) and fluid friction (Figure 14) estimation to be zero. The predicted height of water film increased with the slip ratio and the order of magnitude was in nanometers which is comparable to the order of magnitude of predictions by ATIIM 2.0, however, the model fails to predict the variations in the lateral direction of the contact patch. The average friction coefficient predicted is shown in Figure 15. The predicted order of average friction coefficient according to this model is: **H>F>D>G>A>E>C>B**

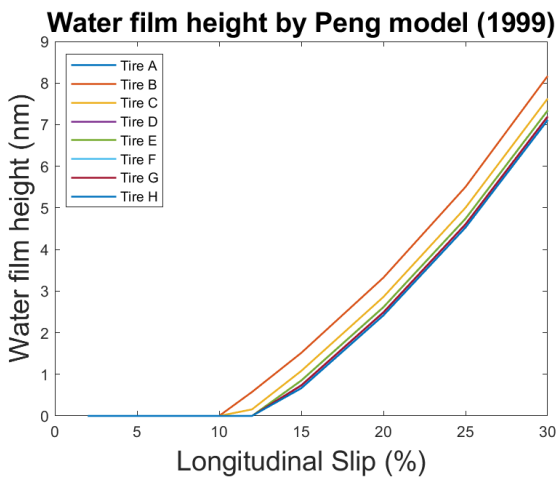

Figure 13: Estimated height of water film varying with the slip in the 1st Peng model

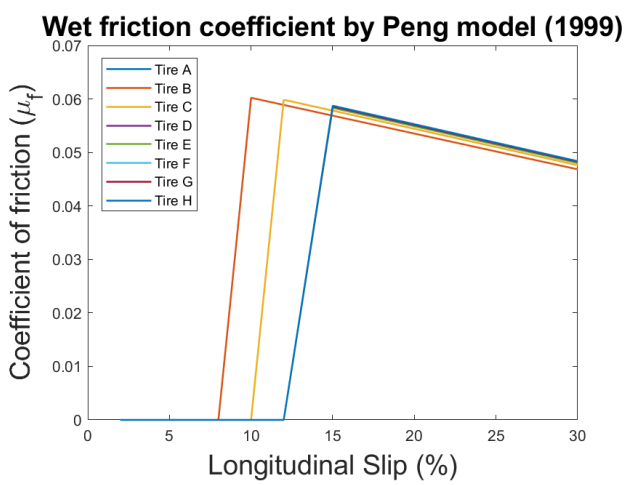

Figure 14: Predicted wet coefficient of friction from 1st Peng model

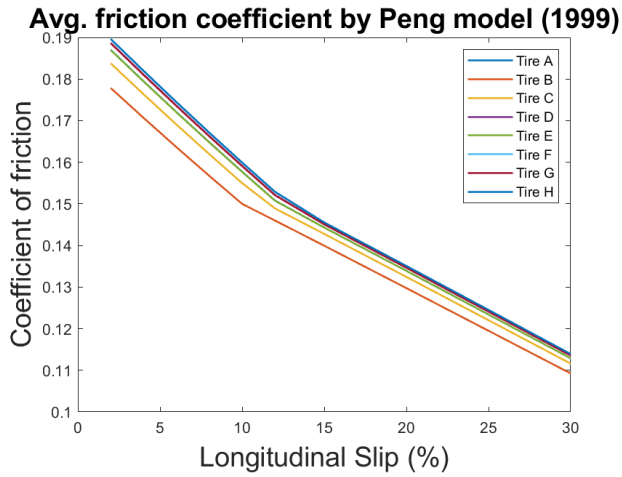

Figure 15: Average coefficient of friction predicted by 1st Peng model

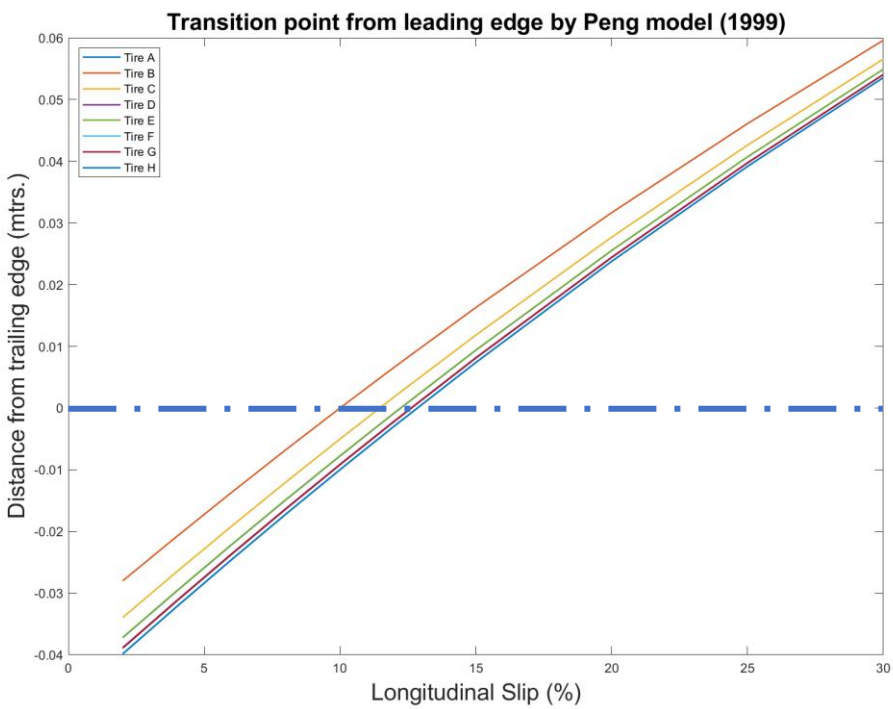

Figure 16: Point of transition variation with slip ratio for all rubber compounds by 1st Peng model

4.6 Discussion on results

Based on the results of the simulations and on comparison with the experimental testing results (Shenvi, 2020; Shenvi et al., 2022) we find that the classical models may have advantages as far as computational effort and simplicity are concerned but fail to round up the complete picture about the tire-ice contact phenomenon. From the perspective of

computation of temperature rise, the ATIIM and ATIIM 2.0 models have the same method and thus the evaluated rise in temperature will be identical. In the results of the simulations for the rise in temperature by the ATIIM model, it was observed that the maximum temperature rise could be considered to occur in the contact patch of tire E1 and tire D1. The evaluated rise in temperature, when greater in magnitude than the bulk ice temperature, by the ATIIM and the classical models can also be an indication of the point at which melting of ice initiates. The Hayhoe and Shapley model tends to overestimate the slip ratio at which melting initiates (20-25%) in comparison to both the Peng et al models as well as ATIIM (8%-12%). This can be considered as a drawback of the Hayhoe and Shapley model. An advantage of the classical friction models beyond the ease of computation and simplicity is the evaluation of the order of total friction coefficient which is the same for all three models i.e. **H>F>D>G>A>E>C>B**. This order of total friction coefficient when compared against the results of the experimental regime (Shenvi et al., 2022), **H>D>B>A>F>E>G>C**, are accurate regarding the evaluation of the best rubber compound. The exact validation of the model friction coefficients by the experimental results would be difficult as the simulation had some assumptions pertaining to material properties of 4 rubber compounds and the constraints in the experimental testing program like the ambient temperature being positive.

Another drawback of all the three classical models is the neglect of the effect of pressure distribution in the lateral direction of the contact patch. By comparing with the simulation results of ATIIM and ATIIM 2.0, we find that in several cases the points along the lateral direction (away from the centerline) saw the maximum temperature rise and height of water film. The assumption of a uniform pressure distribution is another drawback as this does not replicate real conditions and also fails to capture the effect of the tread pattern. In comparison, the predictions of ATIIM and ATIIM 2.0 can be considered to be much better as they successfully capture these effects. ATIIM 2.0 also considers the effect of surface asperities of rubber which may be different even if the tread rubber compound is the same as it can be affected due to the abrasion. ATIIM 2.0 also considers the radii of spherical asperities and their distribution to predict the water film height which will provide a more accurate and realistic prediction, although it is difficult to validate the melted water film experimentally.

5. Conclusions and Future Work

This work focused on simulating the effect of tread rubber compound on the tire performance on ice using a variety of models (2 developed in-house and 3 classical models). Sixteen tires (two per tread rubber compound) were prepared

and then tested in order to measure their pressure distribution in the contact by use of a Tekscan 3150 pressure measurement system. As some material properties pertaining to four rubber compounds were missing, it is difficult to quantify the performance of the models against each other but a qualitative comparison of advantages/disadvantages of the models is attained successfully.

Simulations for the height of water film and rise in temperature were run using ATIIM 2.0 (Mousavi and Sandu, 2020a) and ATIIM (Jimenez and Sandu, 2018) respectively. The temperature rise increased as the tire progressed away from the leading edge of the contact patch and was also significant in the lateral periphery of the contact patch in some cases. The formulations of the three classical models were altered to account for the tread rubber compound properties wherever needed. This helped in highlighting the advantages and disadvantages of these models. A major advantage is the prediction of slip ratio at which melting starts by estimating the position of the transition point. The major drawbacks are the assumption of uniform pressure in the contact patch which does not replicate real-life conditions, and the neglect of the effect of variation of pressure in the lateral direction along with the limited number of properties used for estimation. This leads to a reduction in the reliability of the model predictions although they are able to estimate the best ranked rubber compound in comparison to experimental testing.

Regarding future work, it would be helpful to know all the properties of all the rubber compounds in order to avoid any assumptions and enhance the quality of predictions by ATIIM 2.0. Further, ideally, the measurement of the roughness parameters (input to ATIIM 2.0) needs to be performed after performing the tire break-in. The possibilities of variation in the roughness of ice, the roughness of tread rubber, variation between the points of actual contact, and the actual contact ratio needs to be investigated. The development of a system to measure the contact patch pressure distribution without external aids and at higher resolutions would not only help in measurement of the pressure distribution at higher slip ratios but also in enhancing the quality of predictions of ATIIM 2.0 which could be helpful in investigating the effect of tread rubber.

Acknowledgments

This study has been partially supported by Sumitomo Rubber Industries Ltd. and Terramechanics, Multibody and Vehicle Systems Laboratory at Virginia Tech. The authors would like to thank the guidance and support provided by Dr. Toshio Tada. The authors are grateful to Dr. Rui He, Mr. Adwait Verulkar, Ms. Xiangtong Chen, and Mr. Darshan Rajasekharan for their assistance in the pressure distribution collection.

References

ASTM F1805-20, 2020. Standard Test Method for Single Wheel Driving Traction in a Straight Line on Snow and Ice-Covered Surfaces. ASTM International, West Conshohocken, PA. https://doi.org/10.1520/F1805-20

Bhoopalam, A.K., Sandu, C., Taheri, S., 2016. A tire-ice model (TIM) for traction estimation. J. Terramechanics 66, 1–12. https://doi.org/10.1016/j.jterra.2016.02.003

Bhoopalam, A.K., Sandu, C., Taheri, S., 2014. Tire Traction of Commercial Vehicles on Icy Roads. SAE Int. J. Commer. Veh. 7. https://doi.org/10.4271/2014-01-2292

Blundell, M., Harty, D., 2004. The Multibody Systems Approach to Vehicle Dynamics. Elsevier Butterworth-Heinemann, Burlington, MA.

Evans, D.C.B.., Nye, J.F., Cheeseman, K.J.., 1976. The Kinetic Friction of Ice, in: Proceedings of the Royal Society of London. Series A, Mathematical and Physical Sciences. Royal Society, pp. 493–512.

Fujikawa, T., Funazaki, A., Yamazaki, S., 1994. Tire Tread Temperatures in Actual Contact Areas. Tire Sci. Technol. 22, 19–41.

Hayhoe, G.F., Shapley, C.G., 1989. Tire force generation on ice. SAE Tech. Pap. 98, 30–38. https://doi.org/10.4271/890028

He, R., Jimenez, E., Savitski, D., Sandu, C., Ivanov, V., 2017. Investigating the Parameterization of Dugoff Tire Model Using Experimental Tire-Ice Data. SAE Int. J. Passeng. Cars - Mech. Syst. 10, 83–92. https://doi.org/10.4271/2016-01-8039

Higgins, D.D., Marmo, B.A., Jeffree, C.E., Koutsos, V., Blackford, J.R., 2008. Morphology of ice wear from rubber-ice friction tests and its dependence on temperature and sliding velocity. Wear 265, 634–644. https://doi.org/10.1016/j.wear.2007.12.015

Isitman, N.A., Kriston, A., Fülöp, T., 2017. Role of Rubber Stiffness and Surface Roughness in the Tribological Performance on Ice. Tribol. Trans. 61, 295–303. https://doi.org/10.1080/10402004.2017.1319002

Jimenez, E., Sandu, C., 2018. Towards a real-time pneumatic tire performance prediction using an advanced tire-ice interface model. J. Terramechanics 81, 43–56. https://doi.org/10.1016/j.jterra.2018.04.004

Klapproth, C., Kessel, T.M., Wiese, K., Wies, B., 2016. An advanced viscous model for rubber-ice-friction. Tribol. Int. 99, 169–181. https://doi.org/10.1016/j.triboint.2015.09.012

Lahayne, O., Pichler, B., Reihsner, R., Eberhardsteiner, J., Suh, J., Kim, D., Nam, S., Paek, H., Lorenz, B., Persson, B.N.J., 2016. Rubber Friction on Ice: Experiments and Modeling. Tribol. Lett. 62, 1–19. https://doi.org/10.1007/s11249-016-0665-z

Misiewicz, P.A., Blackburn, K., Richards, T.E., Brighton, J.L., Godwin, R.J., 2015. The evaluation and calibration of pressure mapping system for the measurement of the pressure distribution of agricultural tyres. Biosyst. Eng. 130, 81–91. https://doi.org/10.1016/j.biosystemseng.2014.12.006

Moore, D.F., 1975. The Friction of Pneumatic Tires.

Mousavi, H., Sandu, C., 2020a. Tire-ice model development for the simulation of rubber compounds effect on tire performance. J. Terramechanics 91, 97–115. https://doi.org/10.1016/j.jterra.2020.06.001

Mousavi, H., Sandu, C., 2020b. Study on the Effects of Rubber Compounds on Tire Performance on Ice. SAE Tech.

Pap. 2020-April, 1–9. https://doi.org/10.4271/2020-01-1228

Mousavi, H., Sandu, C., 2020c. Sensitivity analysis of tire-ice friction coefficient as affected by tire rubber compound properties. J. Terramechanics 91, 319–328.

Nakajima, Y., 2019. Advanced Tire Mechanics, Advanced Tire Mechanics. Springer Nature Singapore, Tokyo, Japan. https://doi.org/10.1007/978-981-13-5799-2

Navin, F., Macnabb, M., Nicolletti, C., 1996. Vehicle Traction Experiments on Snow and Ice. SAE Tech. Pap. Ser. 1. https://doi.org/10.4271/960652

Peng, X.D., Xie, Y.B., Guo, K.H., 2000. A new method for determining tire traction on ice, in: SAE Technical Papers. https://doi.org/10.4271/2000-01-1640

Peng, X.D., Xie, Y.B., Guo, K.H., 1999. A tire traction modeling for use in ice mobile. SAE Tech. Pap. 108, 873–880. https://doi.org/10.4271/1999-01-0478

Persson, B.N.J., 2006. Rubber friction: Role of the flash temperature. J. Phys. Condens. Matter 18, 7789–7823. https://doi.org/10.1088/0953-8984/18/32/025

Ripka, S., Lind, H., Wangenheim, M., Wallaschek, J., Wiese, K., Wies, B., 2012. Investigation of Friction mechanisms of siped tire tread blocks on snowy and icy surfaces. Tire Sci. Technol. 40, 1–24. https://doi.org/10.2346/1.3684409

Sandu, C., Taylor, B., Biggans, J., Ahmadian, M., 2008. Building Infrastructure for Indoor Terramechanics Studies: The Development of a Terramechanics Rig at Virginia Tech, in: Proceedings of 16th ISTVS International Conference, Turin, Italy. Turin, Italy.

Shenvi, M.N., 2020. Comparative Study of the Effect of Tread Rubber Compound on Tire Performance on Ice. Virginia Polytechnic Institute and State University.

Shenvi, M.N., Verulkar, A., Sandu, C., Mousavi, H., 2022. Tread rubber compound effect in winter tires: An experimental study. J. Terramechanics 99, 57–73. https://doi.org/10.1016/j.jterra.2021.11.004

Skouvaklis, G., Blackford, J.R., Koutsos, V., 2012. Friction of rubber on ice: A new machine, influence of rubber properties and sliding parameters. Tribol. Int. 49, 44–52. https://doi.org/10.1016/j.triboint.2011.12.015

Tekscan Inc., 2018. Pressure Mapping Sensor 3150 Datasheet 20215.

Tuononen, A.J., Kriston, A., Persson, B., 2016. Multiscale physics of rubber-ice friction. J. Chem. Phys. 145, 1–11. https://doi.org/10.1063/1.4962576

US. Department of Transportation, 2020. US DOT: How do weather events impact roads? [WWW Document]. URL https://ops.fhwa.dot.gov/weather/q1_roadimpact.htm (accessed 6.5.20).

US. Department of Transportation, Administration, F.H., 2020. US DOT Road Weather Management Program [WWW Document]. URL https://ops.fhwa.dot.gov/weather/weather_events/snow_ice.htm (accessed 6.5.20).

Wallaschek, J., Wies, B., 2013. Tyre tread-block friction: modelling, simulation and experimental validation. Veh. Syst. Dyn. 51, 1017–1026.

Wiese, K., Kessel, T.M., Mundl, R., Wies, B., 2012. An analytical thermodynamic approach to friction of rubber on ice. Tire Sci. Technol. 40, 124–150.

Xu, F., Yoshimura, K.I., Mizuta, H., 2013. Experimental study on friction properties of rubber material: Influence of surface roughness on sliding friction. Procedia Eng. 68, 19–23. https://doi.org/10.1016/j.proeng.2013.12.141

Yamazaki, S., Yamaguchi, M., Hiroki, E., Suzuki, T., 2000. Effects of the number of siping edges in a tire tread block on Friction Property and Contact with an Icy Road. Tire Sci. Technol. 28, 58–69.